# Recent ZEUS results

Uwe Schneekloth

Deutsches Elektronen-Synchrotron DESY
Hamburg, Germany

**Abstract**

Recent results from the ZEUS experiment at the HERA $ep$ collider are presented. Differential cross sections for charged current deep inelastic scattering at a center of mass energy of 318 GeV have been measured. The results are in good agreement with Standard Model predictions. Searches for single-top production and lepton flavor violation in $\tau$ production provide new limits on anomalous coupling constants and limits on the mass of leptoquarks. Cross sections for deeply virtual Compton scattering have been measured and compared to QCD-based calculations. Scaling violation has been observed for jet photoproduction. In addition, a precise measurement of the strong coupling constant $\alpha_s(M_Z)$ has been obtained.

# 1 Introduction

The ZEUS detector at the HERA collider, colliding 27.5 GeV electrons (positrons) on 820 and 920 GeV protons, corresponding to center of mass energies of 300 and 318 GeV, has been taking data since 1992. The data samples consist of integrated luminosities of 116 pb$^{-1}$ for $e^+p$ and 17 pb$^{-1}$ for $e^-p$ collisions. A wealth of physics results have been obtained so far. A few selected recent results on deep inelastic scattering, searches for new physics, deeply virtual Compton scattering and jet photoproduction, including a precise measurement of the strong coupling constant $\alpha_s(M_Z)$, are reported in this paper.

# 2 Charged Current Deep Inelastic Scattering

In the Standard Model (SM), charged current (CC) deep inelastic scattering (DIS) is mediated by the exchange of the $W$ boson. In contrast to neutral current (NC) interactions, where all quark and antiquark flavors participate, only down-type quarks and up-type antiquarks participate at leading order in the $e^+p$ CC DIS reaction. Such interactions are, therefore, a powerful tool for flavor-specific investigations of the parton distribution functions (PDFs). Since only left-handed quarks and right-handed antiquarks contribute to CC DIS, the distribution of the positron-quark center-of-mass scattering angle, $\theta^*$, is a sensitive probe of the chiral structure of the weak interaction.

For the reaction $e^+p \to \bar{\nu}_e X$ ($e^-p \to \nu_e X$), the CC DIS differential cross section $d^2\sigma^{\rm CC}_{\rm Born}(e^\pm p)/dxdQ^2$, ($Q^2$ is the negative square of the four-momentum and $x$ the Bjorken scaling variable) can be written at leading order in the electroweak interaction assuming longitudinally unpolarized beams as [1]:

$$\frac{d^2\sigma^{\rm CC}_{\rm Born}(e^\pm p)}{dxdQ^2} = \frac{G_{\rm F}^2}{4\pi x}\frac{M_W^4}{(Q^2+M_W^2)^2}\times \left[Y_+F^{\rm CC}_{2,e^\pm p}(x,Q^2) - y^2F^{\rm CC}_{{\rm L},e^\pm p}(x,Q^2) \mp Y_-xF^{\rm CC}_{3,e^\pm p}(x,Q^2)\right]. \quad (1)$$

In this equation, $G_{\mathrm{F}}$ is the Fermi constant, $M_W$ is the mass of the $W$ boson, $y = Q^2/xs$ (neglecting the masses of the incoming particles) and $Y_{\pm} = 1 \pm (1-y)^2$. The center of mass energy in the positron-proton collisions is given by $\sqrt{s} = 2\sqrt{E_e E_p}$, where $E_e$ and $E_p$ are the positron and proton beam energies, respectively. The inelasticity, $y$, is related to $\theta^*$ by $y = (1-\cos\theta^*)/2$. At leading order in QCD, the structure-functions $F_{2,e^+p}^{\mathrm{CC}}$ and $xF_{3,e^+p}^{\mathrm{CC}}$, may be written in terms of sums and differences of quark and antiquark PDFs of the proton as follows:

$$F_{2,e^+p}^{CC} = x[d(x,Q^2) + s(x,Q^2) + \bar{u}(x,Q^2) + \bar{c}(x,Q^2)], \tag{2}$$

$$xF_{3,e^+p}^{CC} = x[d(x,Q^2) + s(x,Q^2) - \bar{u}(x,Q^2) - \bar{c}(x,Q^2)], \tag{3}$$

where, for example, the PDF $d(x,Q^2)$ gives the number density of down quarks with momentum-fraction $x$ at a given $Q^2$. In case of $e^-p$ instead of $e^+p$ scattering, down-type quark densities are replaced by up–type quark densities and vice versa. The longitudinal structure function, $F_{\mathrm{L},e^+p}^{CC}$, is zero at leading order in QCD.

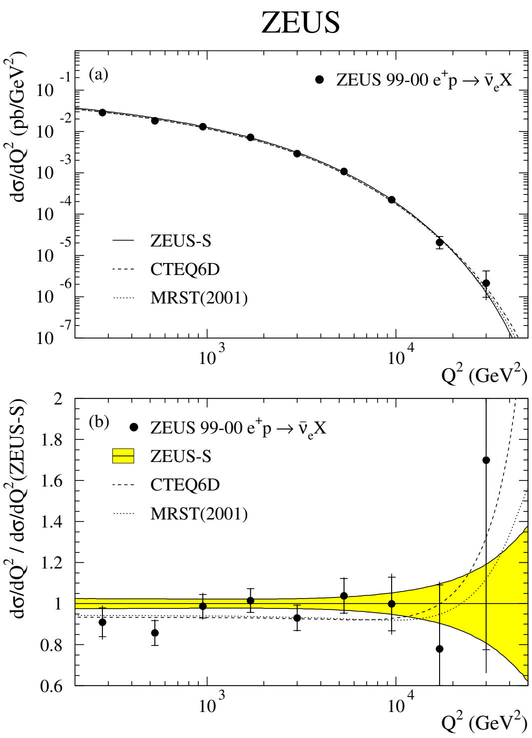


Figure 1: *(a) The $e^+p$ CC DIS Born cross section $d\sigma/dQ^2$ for data and the SM expectation. (b) The ratio of the measured cross section to the SM expectation using the ZEUS-S fit.*

Charged current DIS events were selected by requiring a large missing transverse momentum, $P_{T,miss}$, and a reconstructed event vertex consistent with an $ep$ interaction.

Requirements on the primary vertex and on tracks reconstructed in the central tracking detector were made for central events, where the polar angle of the hadronic system, $\gamma_0$, was greater than 0.4rad. Events were required to satisfy $P_{T,miss} > 20$GeV. For events with $\gamma_0 < 0.4$rad the vertex was determined using calorimeter timing information. The $P_{T,miss}$ criterion was $> 14$ GeV.

The data sample was restricted to $Q^2 > 200\mathrm{GeV}^2$ and $y < 0.9$, where the resolution of the kinematic variables is good and backgrounds are small. The number of events which satisfied all selection criteria were 1164 in the large- and 292 and small-$\gamma_0$ samples.

The luminosity was measured with the ZEUS luminosity monitor [2] using the Bethe-Heitler reaction $ep \to e\gamma p$. The corresponding luminosity was $60.9 \pm 1.4\mathrm{pb}^{-1}$.

The trigger and data selection efficiency and background contribution was estimated using Monte Carlo (MC) generators. Charged current DIS events, including electroweak radiative effects, were simulated using the HERACLES 4.6.1 [3] program with the DJANGOH 1.1 [4] interface. Initial-state radiation, vertex and propagator corrections and two-boson exchange are included in HERACLES. The mass of the $W$ boson was calculated using the PDG [5] values for the fine structure constant, the Fermi constant, the masses of the $Z$ boson and the top quark, and with the Higgs-boson mass set to 100 GeV. The events were generated using the CTEQ5D [6] PDFs.

The measured total cross section for $e^+p$ CC DIS in the kinematic region $Q^2 > 200 GeV^2$ is

$$\sigma_{\rm tot}^{\rm CC}(Q^2 > 200\ {\rm GeV}^2) = 34.8 \pm 0.9({\rm stat.})^{+0.9}_{-1.0}({\rm syst.})\ {\rm pb}. \quad (4)$$

The result is in agreement with the SM expectation of $37.0^{+1.7}_{-0.8}$ pb evaluated using the ZEUS-S fit [7].

The single-differential cross sections $d\sigma/dQ^2$, $d\sigma/dx$ and $d\sigma/dy$ were measured for $Q^2 > 200\ GeV^2$. $d\sigma/dQ^2$ is shown in Fig. 1. The SM cross sections derived from Eq. (1) using the ZEUS-S fit, the CTEQ6D [8] and the MRST(2001) [9] parameterizations of the PDFs are shown, together with the ratios of the measured cross sections to the SM cross section evaluated with the ZEUS-S fit.

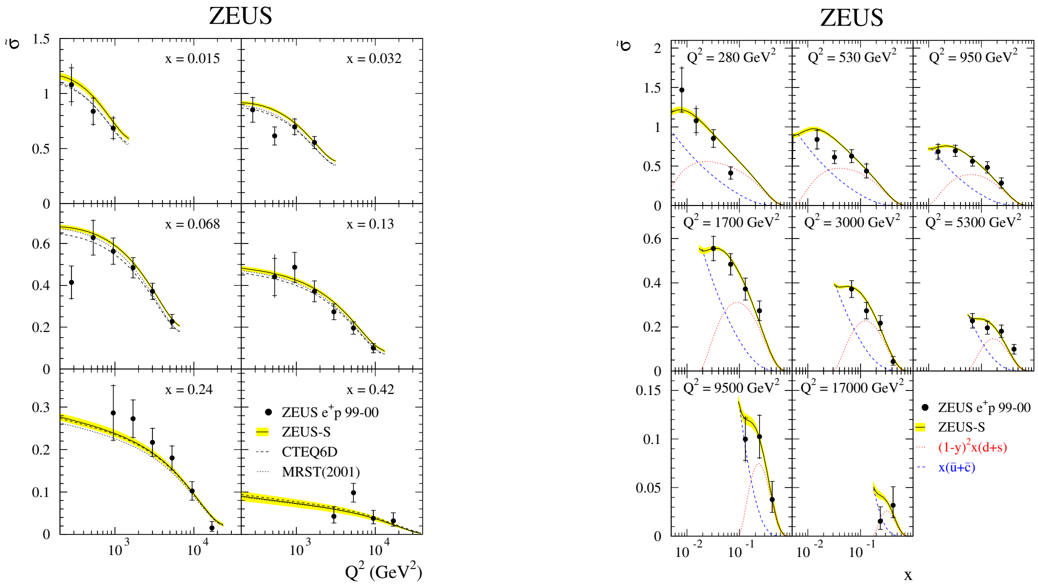


Figure 2: *Left (right) figure: Reduced cross section as a function of $Q^2$ ($x$) for different values of $x$ ($Q^2$) and the SM expectation evaluated using the ZEUS-S, CTEQ6D and MRST(2001) PDF.*

The cross sections $d\sigma/dQ^2$ and $d\sigma/dx$ drop by four and three orders of magnitude, respectively, due to the effect of the $W$-boson propagator and the decreasing quark density at large $x$. The excellent description of the data by the SM prediction based on this fit confirms both the decomposition of the proton momentum into different quark flavors, specifically the down-quark contribution, and the evolution of parton distributions towards scales considerably larger than the $W$-boson mass.

At leading order in QCD, the reduced double-differential cross section,

$$\tilde{\sigma} = \left[\frac{G_F^2}{2\pi x}\Big(\frac{M_W^2}{M_W^2 + Q^2}\Big)^2\right]^{-1} \frac{d^2\sigma}{dxQ^2}, \quad (5)$$

depends on the quark momentum distribution as follows:

$$\tilde{\sigma}(e^+p \to \bar{\nu_2}X) = x[\bar{u} + \bar{c} + (1-y)^2(d+s)]. \quad (6)$$

In Fig. 2 $\tilde{\sigma}$ is shown as a function of $Q^2$ and $x$, respectively. The result is in good agreement with the predictions.

The $W$ boson couples only to left-handed fermions and right-handed antifermions. Therefore, the angular distribution of the scattered quark in $e^+\bar{q}$ CC DIS will be flat in $\theta^*$, while it will exhibit a $(1+\cos\theta^*)^2$ distribution in $e^+q$ scattering. Since $(1-y)^2 \propto (1+\cos\theta^*)^2$, the helicity structure of CC interactions can be illustrated by plotting the reduced double-differential cross section of Eq. (6) versus $(1-y)^2$ in bins of $x$. In the region of approximate scaling, i.e. $x \sim 0.1$, this yields a straight line. At leading order in QCD, the intercept of this line gives the $(\bar{u}+\bar{c})$ contribution, while the slope gives the $(d+s)$ contribution.

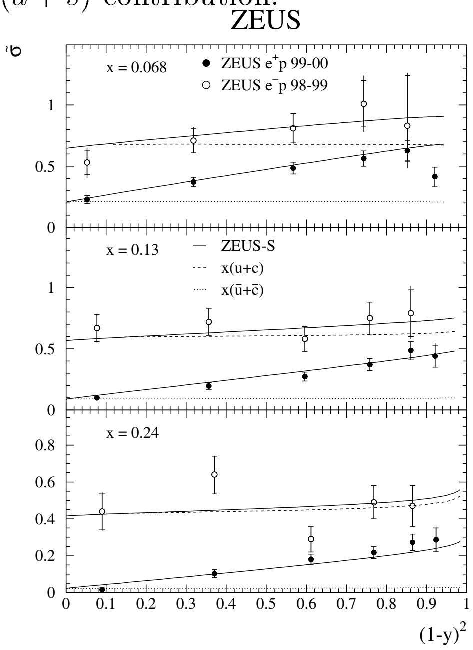


Figure 3: *Reduced cross section as a function of $(1-y)^2$ for different values of $x$ for $e^+p$ and $e^-p$ CC DIS. The expectation of the SM evaluated using the ZEUS-S is shown as a solid line. The contributions of PDF combinations are shown as dashed and dotted lines.*

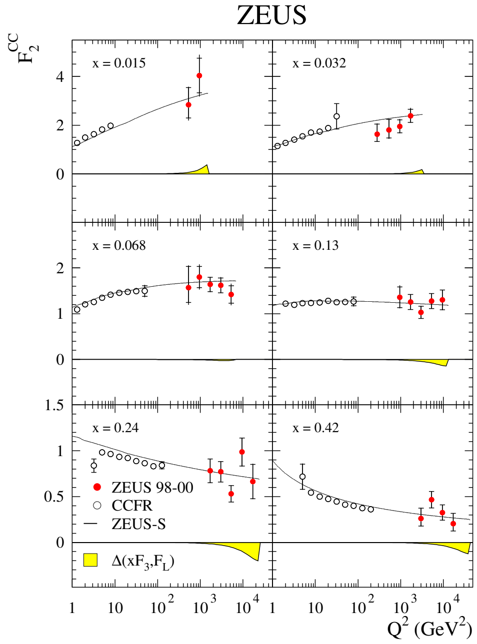


Figure 4: *Structure function $F_2^{CC}$ as a function of $Q^2$, extracted from ZEUS data, compared to CCFR measurements and the expectation of the SM evaluated using the ZEUS-S fit.*

Fig. 3 shows $\tilde{\sigma}$ as a function of $(1-y)^2$ for the $e^+p$ CC DIS data, compared to the previously published $e^-p$ data [10]. At large $x$, $e^+p$ CC DIS is sensitive to the valence part of $d(x,Q^2)$, while $e^-p$ CC DIS is sensitive to the valence part of $u(x,Q^2)$. Equivalently to Eq. (6), the reduced cross section for $e^-p$ CC DIS can be written as

$$\tilde{\sigma}(e^-p \to \nu_e X) = x\left[u + c + (1-y)^2(\bar{d}+\bar{s})\right], \quad (7)$$

permitting a similar interpretation for the intercept and slope in terms of the appropriate parton densities. Scaling violations can be observed in the theoretical prediction as $(1-y)^2$ approaches one. The data agree with the expectation of the SM from the ZEUS-S fit.

The structure function $F_2^{CC}$ can be obtained by combining the measurements presented in this paper with the previous ZEUS $e^-p$ CC DIS results [10]. Using Eq. (1), the sum of $F_{2,e^+p}^{CC}$ and $F_{2,e^-p}^{CC}$ can be extracted from the measured CC cross sections as:

$$F_2^{\mathrm{CC}} = \frac{4\pi x}{G_F^2}\left(\frac{M_W^2+Q^2}{M_W^2}\right)^2 \frac{1}{Y_+}\left(\frac{d^2\sigma_{Born}^{\mathrm{CC}}(e^+p)}{dxdQ^2}+\frac{d^2\sigma_{Born}^{\mathrm{CC}}(e^-p)}{dxdQ^2}\right)+\Delta(xF_3,F_{\mathrm{L}}), \quad (8)$$

where $\Delta(xF_3, F_{\mathrm{L}})$ is a correction term taking into account the $xF_3$ and $F_L$ structure functions. Fig. 4 shows the extracted structure-function $F_2^{\mathrm{CC}}$ as a function of $Q^2$ for different values of $x$. The size of the correction $\Delta(xF_3, F_{\mathrm{L}})$, computed at NLO in QCD using the ZEUS-S fit, is shown as a shaded area in each bin. The data are well described by the SM prediction.

# 3 Search for new Physics

Extensive searches for new physics beyond the SM have been performed by the ZEUS collaboration. Two recent results are reported, the search for single-top quark production and searches for lepton flavor violation in $\tau$ production.

## 3.1 Single-top Production

Observables sensitive to flavor-changing neutral current (FCNC) interactions are particularly useful as probes for physics beyond the SM, since SM rates are very small due to the GIM mechanism. At the HERA collider, single-top production is a prime reaction to search for FCNC, where the incoming lepton exchanges a $\gamma$ or $Z$ with an up-type quark in the proton, producing a top quark in the final state. Deviations from the SM can be parameterized in terms of coupling constants $\kappa_{tu\gamma}$, $v_{tuZ}$ described by an effective Lagrangian of [11]

$$\Delta\mathcal{L}_{eff} = ee_t\bar{t}\frac{i\sigma_{\mu\nu}q^\nu}{\Lambda}\kappa_{tu\gamma}uA^\mu + \frac{g}{2\cos\theta_W}\bar{t}\gamma_\mu v_{tuZ}uZ^\mu + h.c. \quad (9)$$

In a previous ZEUS publication, single-top production was simulated using the HEXF generator [12]. For this analysis, the process $eu \to et$ was simulated using the COMPHEP generator[13], including a full simulation of the $\gamma-$ and $Z-$ exchange processes. The proton remnant, initial and final state QED and QCD radiation, hadronization and particle decays were simulated by PYTHIA6 [14].

The top quark search was optimized for the decay $t \to bW^+$, both leptonic and hadronic $W$ decays were considered. The data sample corresponds to an integrated luminosity of 130.1 $pb^{-1}$ at $\sqrt{s}$ of 300 and 318 GeV. Events with missing momentum and isolated high energy lepton ($e$ or $\mu$) or with 3 high energy jets, in case of leptonic or hadronic $W$ decays, were selected. Details of the analysis can be found in [15]. No event was found in the leptonic channel after the final cuts. In the hadronic channel the number of observed events was as expected from the SM prediction. As a result limits at 95% confidence level on the magnetic $\kappa_{tu\gamma}$ and vector couplings $v_{tuZ}$ were obtained, see Fig. 5. The limit on $\kappa_{tu\gamma}$ was improved considerably compared to the LEP [16] and CDF [17] results.

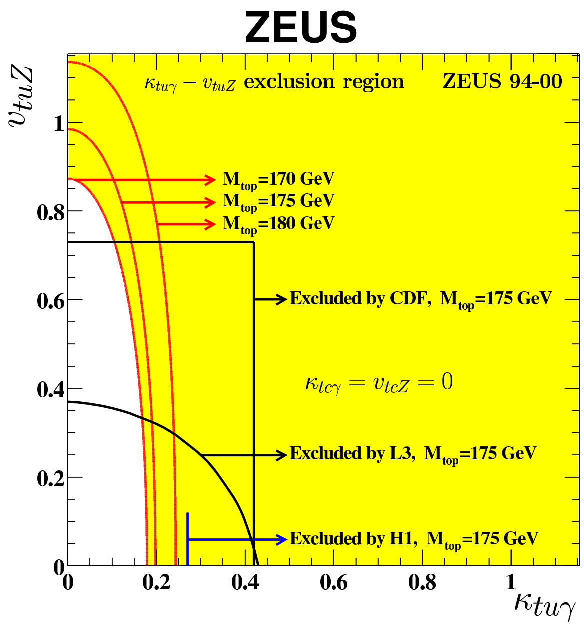


Figure 5: *Exclusion regions at 95% CL in the $\kappa_{tu\gamma} - v_{tuZ}$ plane for three values of $M_{top}$ assuming $\kappa_{tc\gamma} - v_{tcZ} = 0$.*

## 3.2 Search for tau Flavor Violation

There are several extensions of the SM, which predict sizeable rates of lepton-flavor-violation (LFV). At HERA, reactions like $eq_i \to \tau q_f$ can be mediated by leptoquarks (LQs), bosons that carry both lepton and baryon quantum numbers and have lepton-quark Yukawa couplings. These reactions can also occur through the exchange of squarks in R-parity-violating SUSY models.

Previous searches for LFV at HERA have been performed looking for muons in the final state. In this analysis a search for the process $e^+p \to \tau X$ is performed. The Buchmüller-Rückl-Wyler (BRW) model [18] is used in order to classify the LQs and to calculate the cross sections.

The event signature is a high transverse momentum isolated $\tau$ balanced by a jet. There is a large transverse momentum imbalance, since only the $\tau$ decay products are observed in the detector. An isolated $e$ or $\mu$ was required for the leptonic channel, 35% of all decays. For the hadronic decay channels, a $\tau$ discriminant was defined, making use of the narrow jet-like $\tau$ decay characteristics. Details of the analysis are described in [19] .

No candidate event was found in any channel, in good agreement with the prediction for SM processes (CC DIS, di-muon and di-tau production in photon-photon interactions or photoproduction) of $0.8 \pm 0.3$ events.

For LQs with mass less than $\sqrt{s}$, limits at the 95% C.L. on $\lambda_{eq_1}\sqrt{\beta_{\tau q}}$ were derived for $F = 0$ LQs, where $\lambda_{eq_1}$ is the coupling of the LQ to an electron and a first generation quark $q_1$ and $\beta_{\tau q}$ is the branching ratio of the LQ to $\tau$ and a quark $q$. $F$ is the LQ fermionic number. Figures 6(a-b) show the upper limits on $\lambda_{eq_1}\sqrt{\beta_{\tau q}}$ for scalar and vector LQs. Limits on $\lambda_{eq_1}$ are derived assuming $\lambda_{eq_1} = \lambda_{\tau q_\beta}$ for $\tilde{S}^L_{1/2}$ and $V^R_0$ LQs. The limits

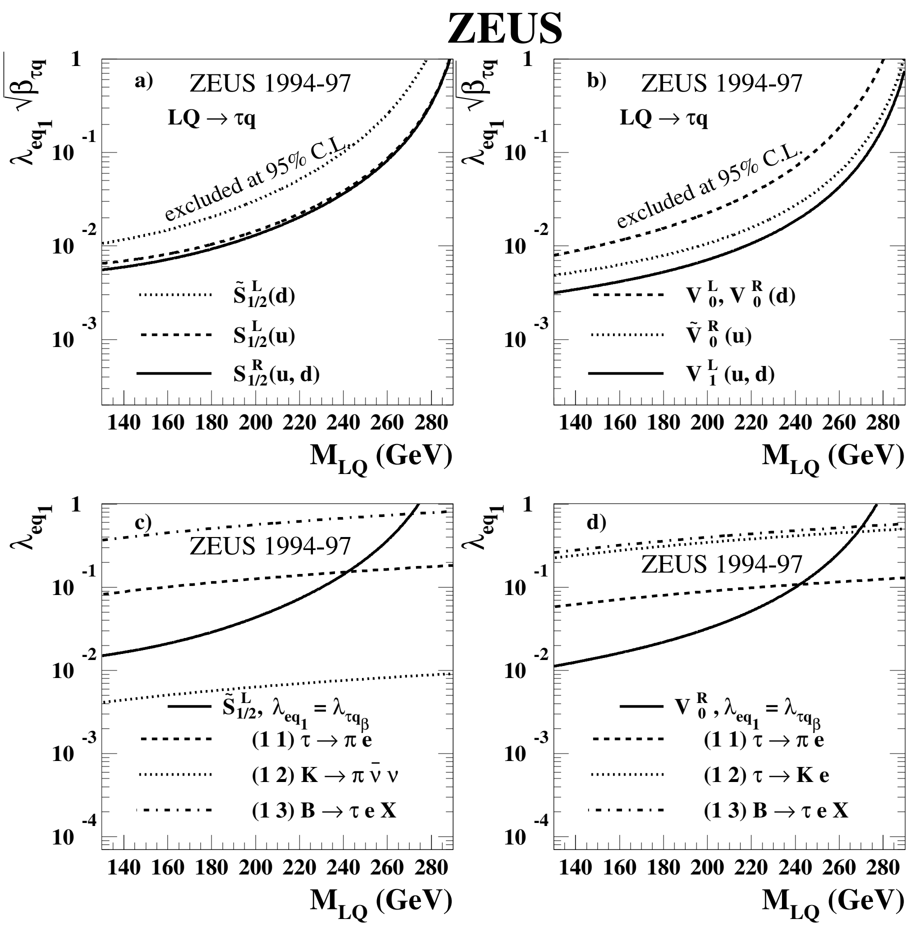


Figure 6: *Upper limits at 95% C.L. on* $\lambda_{eq_1}\sqrt{\beta_{\tau q}}$ *vs.* $M_{LQ}$ *for a) scalar and b) vector LQs. Upper limits on* $\lambda_{eq_1}$ *assuming* $\beta_{\tau q} = 0.5$ *for c) scalar and d) vector LQs that couple to d-type quarks.*

on $\lambda_{eq_1}\sqrt{\beta_{\tau q}}$ for $\tilde{S}^L_{1/2}$ also apply as limits on $\lambda'_{1j1}\sqrt{\beta_{\tilde{u^j}\to\tau q}}$ for $\tilde{u^j}$ squarks. Assuming that the couplings have electromagnetic strength ($\lambda_{eq_1} = \lambda_{\tau q_\beta} = 0.3$), LQs with masses up to 299 GeV are excluded at 95%C.L.

# 4 Deeply Virtual Compton Scattering

The exclusive production of a real photon in diffractive $ep$ interactions, $ep \to e\gamma p$, is known as deeply virtual Compton scattering (DVCS) [20, 21, 22, 23]. This process is calculable in perturbative QCD when the virtuality of the exchanged photon is large. DVCS can be used to study the proton structure by measuring correlations between pairs of gluons within the proton. Correlations are parameterized by generalized parton distribution functions (GPD) [23, 24, 25], which provide information about the wave function of the proton.

The advantage of studying DCVS is the simple state and absence of hadronization. QCD predictions are, therefore, more reliable than for many other exclusive final states. It is one of the best understood exclusive processes in $ep$.

In this analysis, the dependence of the DVCS cross section on $W$, the center of mass of the virtual photon-proton system, and $Q^2$ is studied in the kinematic range $5 < Q < 100 GeV^2$ and $40 < W < E140GeV$. The measurements are integrated over $t$, the square of the four-momentum transfer at the proton vertex. The first measurement of the $e^-p$ cross section is reported.

The experimental signature, a photon and the scattered electron with balanced transverse momenta, is similar to those of the purely electromagnetic Bethe-Heitler (BH) process. Two isolated electromagnetic clusters were required in the calorimeter. The first one EM1 in the RCAL with $E_1$ >15 GeV and the second EM2 either in the RCAL with $E_2$ >3 GeV or in the BCAL with $E_2$ >2.5 GeV. Photoproduction background was rejected by a cut on the difference of total energy and longitudinal momentum.

The events were subdivided into three samples: The $\gamma$ sample: EM2 with no track (photon candidate), and EM1 is the scattered-electron candidate. Both BH and DVCS processes contribute to this topology. The $e$ sample: EM2 with the right-charge track (scattered-electron candidate) and EM1 is the photon candidate. This sample is dominated by the BH process. The contribution from DVCS is negligible. The wrong-sign-$e$ sample: EM2 with wrong-charge-sign track. This background sample is due to non-resonant $e^+e^-$ production or to $J/\Psi$ production and subsequent decay. The wrong-sign-$e$ sample was used to statistically subtract the background contributions to the $e$ sample in each kinematic bin.

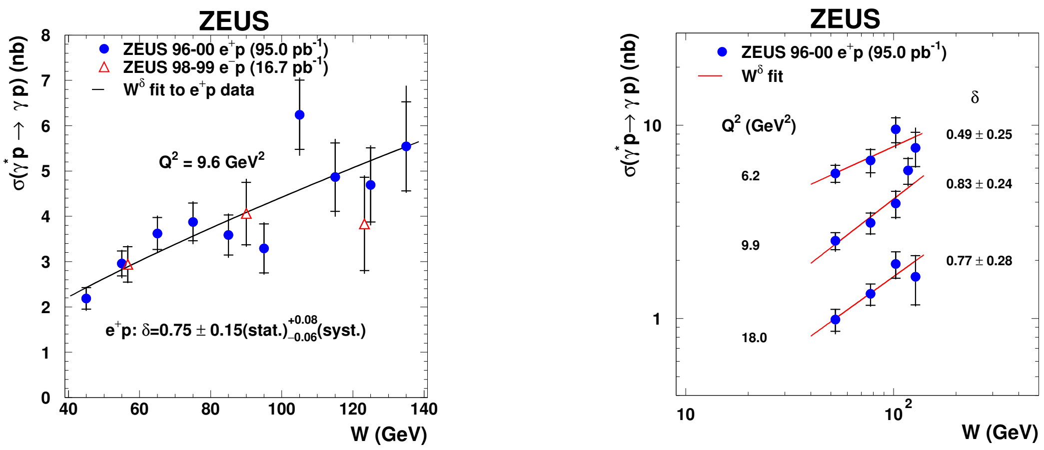


Figure 7: *The DVCS cross section, $\sigma(\gamma^\star p \to \gamma p)$, as a function of W: left figure for an average $Q^2 = 9.6GeV^2$, right figure for three $Q^2$ values. The solid line is the results of a fit of the form $\sigma_{DVCS} \propto W^\delta$.*

The DVCS signal was extracted from the $\gamma$ sample by subtracting the BH background. BH events were simulated using the GRAPE-Compton and GRAPE-Dilepton generators[31]. The normalization of the MC was determined from the wrong-sign-$e$ sample

The GenDVCS MC generator[26], based on a model by Frankfurt, Freund and Strikman (FFS) [23], was used to simulate the elastic DVCS process. In the FFS calculation, the DVCS cross-section is related to the inclusive structure-function $F_2$ through

$$\frac{d^3\sigma_{DVCS}^{ep\to e\gamma p}}{dxdQ^2dt} = \frac{\pi^2\alpha^3}{2xR^2Q^6}[1+(1-y)^2]e^{-b|t|}F_2^2(x,Q^2)(1+\rho^2), \tag{10}$$

where $x \simeq Q^2/(Q^2+W^2)$ is the Bjorken scaling variable, $b$ is the exponential slope of the $t$ dependence and $y$ is the fraction of the electron energy transferred to the proton in its rest frame. The ratio $R = \Im m\mathcal{A}(\gamma^\star p \to \gamma^\star p)|_{t=0}/\Im m\mathcal{A}(\gamma^\star p \to \gamma p)|_{t=0}$ accounts for the non-forward character of the DVCS process and is directly related to a ratio of the GPD to the parton distribution functions [30] and is the ratio of the real to imaginary part of the amplitude, $\rho = \Re e\mathcal{A}(\gamma^\star p \to \gamma p)|_{t=0}/\Im m\mathcal{A}(\gamma^\star p \to \gamma p)|_{t=0}$. The value of $R$ is about 0.55, with little dependence on $x$ or $Q^2$ [23]. $\rho$ was parameterized as $\rho = \frac{\pi}{2}(0.176+0.033\ln Q^2)$ ($Q^2$ in GeV)[26].

The W dependence of the DVCS cross-section, $\sigma_{DVCS} = \sigma(\gamma^\star p \to \gamma p)$, for $Q^2 = 9.6$ GeV$^2$ is shown in Fig.7, separately for $e^+p$ and $e^-p$ interactions. Due to the limited statistics, the $e^-$ sample is only shown in three $W$ bins. There is agreement between the two samples.

A fit of the form $\sigma_{DVCS} \propto W^\delta$ was performed separately for the positron and electron data. For the $e^+p$ data, the value $\delta = 0.75 \pm 0.15(stat.)^{+0.08}_{-0.06}(syst.)$ is comparable to that determined for $J/\Psi$ electroproduction [33]. This steep rise in the cross-section is a strong indication of the presence of a hard underlying process. The same fit to the $e^-p$ data yields $\delta = 0.45 \pm 0.36(stat.)^{+0.08}_{-0.07}(syst.)$, which is compatible with the $e^+p$ result.

The positron sample was further subdivided into three $Q^2$ ranges. The $W$ dependence of $\sigma_{DVCS}$ in these three $Q^2$ bins is presented in Fig.7. The results are compatible with no dependence on $Q^2$ although also with the increase with $Q^2$ observed in exclusive production of light vector mesons [32, 34].

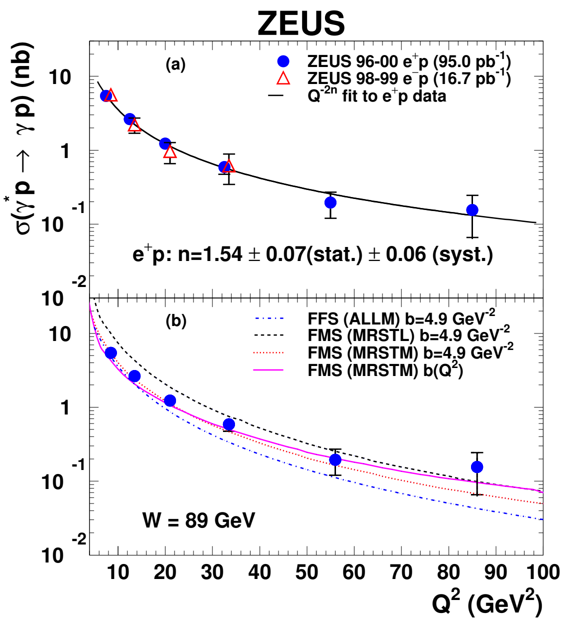


Figure 8: *(a) The DVCS cross section, $\sigma(\gamma^\star p \to \gamma p)$, as a function of $Q^2$ for $W = 89$ GeV, separately for $e^+p$ and $e^-p$ data. The solid line is the results of a fit of the form $\sigma_{DVCS} \propto Q^{-2n}$ to the positron data. (b) $\sigma(\gamma^\star p \to \gamma p)$ is compared to the GPD-based theoretical predictions of FFS and FMS.*

The $Q^2$ dependence of $\sigma_{DVCS}$, for $W = 89$ GeV, is shown in Fig. 8a, again separately for $e^+p$ and $e^-p$ interactions. There is no significant cross-section difference between the $e^+$ and $e^-$ data, which is consistent with the assumption that the present measurement is insensitive to the interference term.

A fit of the form $Q^{-2n}$ to the $e^+p$ data gives a value of $n = 1.54 \pm 0.07(stat.) \pm 0.06(syst.)$. This value is lower than $n \simeq 2$ which is characteristic of exclusive vector-meson production [32, 35]. The fit to the $e^-p$ data gives $n = 1.69 \pm 0.21(stat.)^{+0.09}_{-0.06}(syst.)$.

Freund, McDermott and Strikman (FMS) [30] have made an attempt to model the GPD based on DVCS data [27, 28, 29]. A comparison of DVCS as a function of $Q^2$ for fixed $W$ with the predictions based on the MRST parameterization of the parton distribution functions (PDF) [36, 37] is shown in Fig.8(b). Three FMS curves are shown.

Two curves show the results of modeling based on LO (MRSTL) and NLO (MRSTM) parton distribution functions. The latter leads to predictions closer to the data. In this comparison, a fixed value of the $t$ slope, $b = 4.9$ GeV$^{-2}$, was assumed. The third curve, shown in the figure, corresponds to predictions based on MRSTM, assuming a $Q^2$-dependent $b$ value. The best agreement between the data and the predictions is achieved using $b = 8(1-0.15\ln(Q^2/2))$ GeV$^{-2}$, a parameterization obtained by Freund, McDermott and Strikman [30] from a fit to a preliminary version of the present data.

# 5 Jet-Production in Photoproduction

Jet production can be used as stringent tests of QCD. The comparison of jet cross sections for the same reaction at different center of mass energies allows to study scaling violation and the determination of the strong coupling constant $\alpha_s$.

In the parton model, the scaled invariant jet cross section is independent of the center of mass energy, whereas QCD predicts non-scaling behavior due to the evolution of the structure functions of colliding hadrons and the running of $\alpha_s$.

In photoproduction at HERA, two types of QCD processes contribute to jet production: the photon interacting directly with a parton in the proton (direct process) or the photon acts as a source of partons, one interacting with a parton in the proton (indirect process). Scaling violations should be observed in both processes. In addition, the measurement of the high $E_T^{jet}$ jet cross section over a wide range of $E_T^{jet}$ allows a determination of $\alpha_s$ as well as its energy dependence. Details of the analysis can be found in [38].

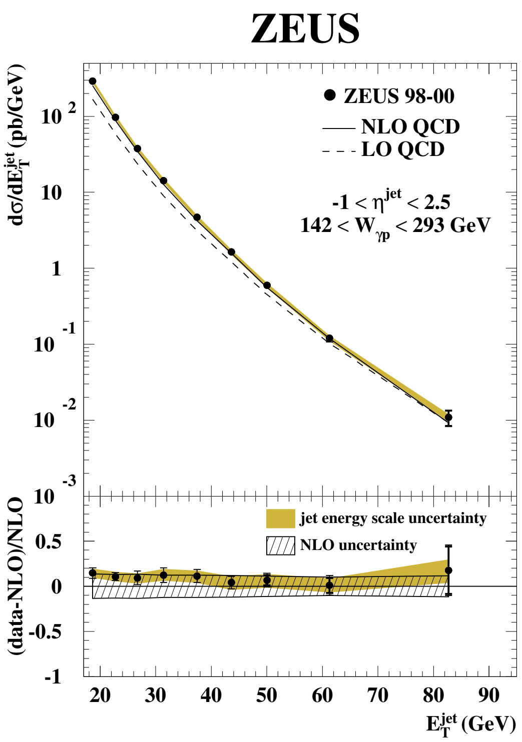


Figure 9: *(a) Measured inclusive jet cross section, $d\sigma/dE_T^{jet}$ (dots) compared to LO (dashed line) and NLO (solid line) QCD parton-level calculations corrected for hadronization effects. (b) The fractional difference between the measured $d\sigma/dE_T^{jet}$ and the NLO QCD calculation; the hatched band shows the uncertainty of the calculation.*

Events with at least one jet with $E_T >$ 10 GeV and $\eta < 2.5$ were accepted at the trigger level. After event vertex and tracking requirements the background from beam-gas interactions, cosmic-ray showers and beam-halo muons was negligible. Charged current DIS events were rejected requiring the missing transverse momentum small compared to the total transverse energy. Neutral current DIS events with an identified scattered electron were removed from the sample. The remaining background was below 0.3%.

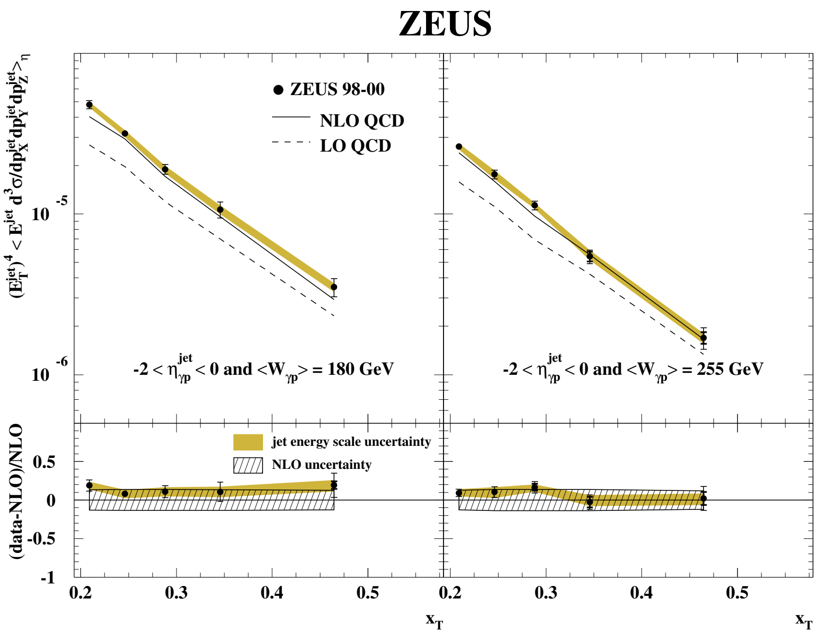


Figure 10: *(a) Measured scaled jet cross section, $(E_T^{jet})^4 < E^{jet} d^3/dp_X^{jet} dp_Y^{jet} dp_Z^{jet} >$, averaged over $-2 < \eta_{\gamma p}^{jet} < 0$ , as a function of $x_T$ (dots) for (a) $< W_{\gamma p} >= 180 GeV$, (b) $< W_{\gamma p} >= 255 GeV$.*

For the analysis the longitudinally-invariant $k_T$ cluster algorithm [39] was used in the inclusive mode [40] to reconstruct jets in the hadronic final state from the energy deposits in the CAL cells. The jet variables were defined according to the Snowmass convention [41]. The jets reconstructed from the CAL cell energies are called calorimetric jets and the variables associated with them are denoted by $E_{T,cal}^{jet}$, $\eta_{cal}^{jet}$ and $\phi_{cal}^{jet}$. A total of about 200000 events with at least one jet satisfying $E_{T,cal}^{jet} > 13$ GeV and $-1 < \eta_{cal}^{jet} < 2.5$ were selected. The $\gamma p$ center of mass energies were restricted to $142 < W < 293$GeV.

The PYTHIA 6.1 [42] and HERWEG 5.9 [43] MC programs were used to generate resolved and direct photoproduction events. The partonic processes were simulated using leading order matrix elements, with initial and final state parton showers. The fragmentation into hadrons was done using the Lund string model [44] in the case of PYTHIA and a cluster model [45] in case of HERWIG.

The QCD calculation, at both leading order (LO) and next-to-leading order (NLO) QCD calculations, are based on a program by Klasen, Kleinwort and Kramer[46]. The MRST99[47] parameterizations of the parton PDFs and the GRV[48] parameterizations for the photon were used for the comparison with the measured cross sections.

Inclusive jet differential cross sections were measured for $142 < W_{\gamma p} < 293$ GeV, jets with $E_T^{jet} > 17$ GeV and $-1 < \eta^{jet} < 2.5$. $d\sigma/dE_T^{jet}$, measured in the $E_T^{jet}$ range between 17 and 95 GeV, are presented in Fig.9. The cross section decreases by over five orders of magnitude in this $E_T^{jet}$ range. The LO QCD calculation underestimate the measured cross section by about 50% for $E_T^{jet} < 45$GeV. Including NLO QCD calculations, the data are well described over the complete $E_T^{jet}$ range.

Fig.10 shows the scaled jet invariant cross section,

$$(E_T^{jet})^4 \left\langle \frac{E^{jet} d^3\sigma}{dp_X^{jet} dp_Y^{jet} dp_Z^{jet}} \right\rangle_\eta, \tag{11}$$

averaged over the range $-2 < \eta_{\gamma p}^{jet} < 0$, as a function of $x_T$ for $< W_{\gamma p} >$ values of 180 and 255 GeV. The LO QCD calculation is again too low, whereas NLO gives a good description of the data.

To test the scaling hypothesis, the ratio of the scaled jet invariant cross sections as a function of $x_T$ was measured for the two chosen values of $< W_{\gamma p} >$, after correcting for the difference in the photon flux [50] between these intervals. Fig.11 shows the measured ratio as a function of $x_T$. It shows a clear deviation from unity, in agreement with the NLO QCD predictions, which include the running of $\alpha_s$ and the evolution of the PDFs with the scale. The evolution causes the predicted ratio to change non-monotonically with $x_T$. The deviation from unity constitutes the first observation of scaling violations in $\gamma p$ interactions.

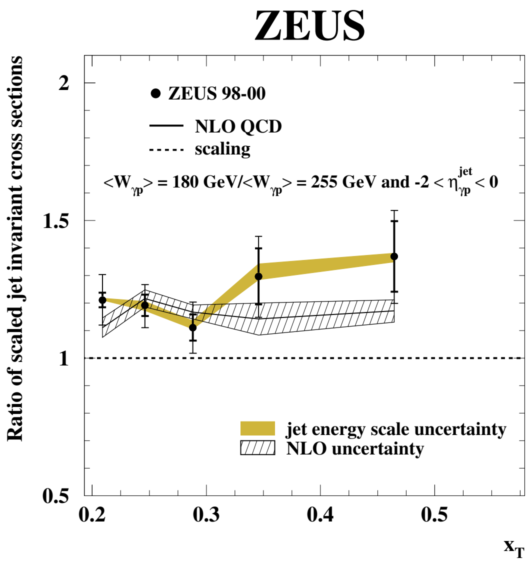


Figure 11: *Measured ratio of scaled jet invariant cross sections, after correcting for the difference in the photon flux between the two $W_{\gamma}p$ intervals, as a function of $x_T$ (dots). The dashed line is the scaling expectation.*

The $\alpha_s(M_Z)$ dependence of the predicted $d\sigma/dE_T^{jet}$ was parameterized according to

$$\left[\frac{d\sigma}{dE_T^{jet}\alpha_s(M_Z)}\right]_i = C_1^i\alpha_s(M_Z)+C_2^i\alpha_s^2(M_Z), \tag{12}$$

where $C_1^i$ and $C_2^i$ are constants, by using the NLO QCD calculations corrected for hadronization effects. The values of $\alpha_s(M_Z)$ as determined from the measured $d\sigma/dE_T^{jet}$ in each region of $E_T^{jet}$ are shown in Fig. 12a.

The largest contribution to the experimental uncertainty comes from the jet energy scale and amounts to $\pm1.5\%$ on $\alpha_s(M_Z)$. The theoretical uncertainties are dominated by terms beyond NLO calculations, which was estimate to $^{+4.2}_{-3.3}\%$. The change of $\alpha_s(M_Z)$ due to the uncertainties on the photon and proton PDFs and on the hadronization corrections were +0.7%,±0.9% and +0.8%, respectively. The total theoretical uncertainty was obtained by adding these uncertainties in quadrature.

By combining all the $E_T^{jet}$ regions, the following value of $\alpha_s(M_Z)$ is obtained:
$\alpha_s(M_Z) = 0.1224 \pm 0.0001(stat.)^{+0.0022}_{-0.0019}(exp.)^{+0.0054}_{-0.0042}(th.)$.

This value of $\alpha_s(M_Z)$ is consistent with the current world average [49] of $0.1183 \pm 0.0027$ as well as with recent determinations from jet production in NC DIS at HERA [51, 52] and collisions at Tevatron [53]. It has a precision comparable to the values obtained from $e^+e^-$ interactions [49].

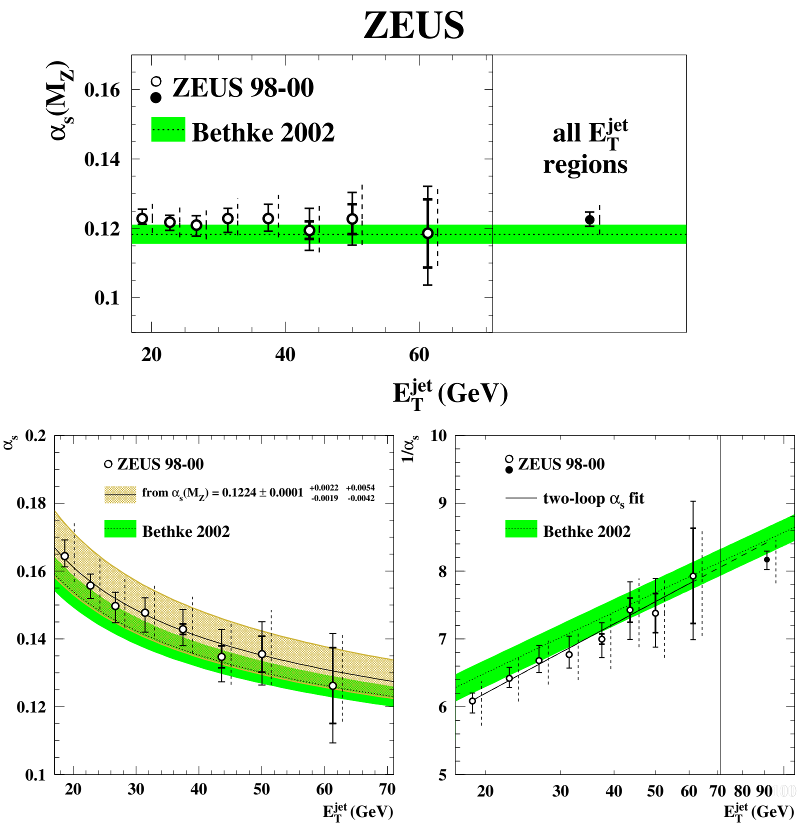


Figure 12: *(a) $\alpha_s(m_Z)$ determined from the QCD fit of the measured $d\sigma/dE_T^{jet}$ in different $E_T^{jet}$ regions (open circles). (b) $\alpha_s(< E_T^{jet} >)$ as a function of $E_T^{jet}$. The solid line represents the prediction of the renormalization group equation obtained from the $\alpha_s(m_Z)$ central value; the logh-shaded area displays its uncertainty. (c) $1/\alpha_s(< E_T^{jet} >)$ as a function of $E_T^{jet}$. The solid line represents the two-loop $\alpha_s$ fit to the mearsured values. The dashed line shows the extrapolation of the result of the fit to $E_T^{jet} = M_Z$.*

The QCD prediction for the energy-scale dependence of the strong coupling constant was explicitly tested by determining $\alpha_s$ from the measured $d\sigma/dE_T^{jet}$ at different $E_T^{jet}$ values. The method employed was the same as described above, but parameterizing the $\alpha_s$ dependence of $d\sigma/dE_T^{jet}$ in terms of $\alpha_s(< E_T^{jet} >)$ instead of $\alpha_s(M_Z)$, where $< E_T^{jet} >$ is the weighted mean of $E_T^{jet}$ in each bin. The measured $\alpha_s(E_T^{jet})$ values are shown in Fig. 12(b). The results are in good agreement with the predicted running of the strong coupling constant over a large range in $E_T^{jet}$.

Fig. 13 shows the result of this analysis, the first measurement of $\alpha_s(m_Z)$ in photoproduction, together with other ZEUS measurements and the world average[49]. All measurements are consistent. The error of the photoproduction result is relatively small. Progress on the theoretical predictions will be essential to match the experimental errors.

Figure 13: *Comparison of recent ZEUS $\alpha_s(m_Z)$ measurements with the world average[49].*

# 6 Acknowledgements

I would like to thank the organizers for a very stimulating conference and a memorable trip on the Volga river. I am grateful to J. Butterworth for a critical reading of the manuscript.

# References

[1] A.M. Cooper-Sarkar, R.C.E. Devenish and A. De Roeck, Int. J. Mod. Phys. **A 13** (1998) 3385

[2] J. Andruszków et al., Preprint DESY-92-066, DESY, 1992;
ZEUS Collaboration, M. Derrick et al., Z. Phys. **C 63** (1994) 391;
J. Andruszków et al., Acta Phys. Pol. **B 32** (2001) 2025

[3] A. Kwiatkowski, H. Spiesberger and H.-J. Möhring, Comp. Phys. Comm. **69** (1992) 155;
H. Spiesberger, *An Event Generator for ep Interactions at HERA Including Radiative Processes (Version 4.6)*, 1996, available on `http://www.desy.de/~hspiesb/heracles.html`.

[4] H. Spiesberger, HERACLES *and* DJANGOH*: Event Generation for ep Interactions at HERA Including Radiative Processes*, 1998, available on `http://www.desy.de/~hspiesb/djangoh.html`.

[5] Particle Data Group, D.E. Groom et al., Eur.Phys.J.C15 (2000) 1

[6] CTEQ Collaboration, H.L. Lai et al., Eur. Phys. J. **C 12** (2000) 375

[7] ZEUS Collaboration, S.Chekanov et al., Phys. Rev. D 67 (2003) 012007

[8] J. Pumplin et al., JHEP **07** (2002) 012

[9] A.D. Martin et al., Eur. Phys. J. **C23** (2002) 73

[10] ZEUS Collaboration, S.Chekanov et al., Phys. Lett. B 539 (2002) 197. Erratum: Phys. Lett. B 552 (2003) 308

[11] T.Han and J.L.Hewett, Phys.Rev. D60 (1999) 074015

[12] H.J.Kim and S.Kartik, Preprint LSUHE-145-1993, 1993.

[13] A.Pukhov et al., Preprint INP-MSU-98-41-542, 1999 also hep-ph/9908288, 1999.

[14] M.Bengtsson and T.Sjöstrand, Comp.Phys.Comm. 46 (1987) 43

[15] ZEUS Collaboration, S.Chekanov et al., Phys. Lett. B 559 (May 2003) 153 - 170.

[16] ALEPH Collaboration, R.Barate et al. Phys.Lett. B 494 (2000) 33;
ALEPH Collaboration, A.Heister et al. Phys.Lett. B 543 (2002) 173;
OPAL Collaboration, G.Abbiendi et al. Phys.Lett. B 521 (2001)181;
L3 Collaboration, P.Achard et al. Phys.Lett. B 549 (2002) 290

[17] CDF Collaboration, F. Abe et al., Phys Rev. Lett. 80 (1998) 2525

[18] W.Buchmüller, R.Rückl and D.Wyler, Phys.Lett. B 191 (1987) 442. Erratum: Phys.Lett. B 448 (1999) 320

[19] ZEUS Collaboration, Search for lepton-flavor violation in $\tau$ production in ep collisions at HERA. Abstract 498, Int.Europhysics Conf. on HEP, Aachen 2003.

[20] E. Wieczorek, V.A. Matveev and D. Robaschik. Theor. Math. Phys. 19 (1974) 315
J. Bartels and M. Loewe. Z. Phys. C 12 (1982) 263
X. Ji. Phys. Rev. D 55 (1997) 7114

[21] A.V. Radyushkin. Phys. Rev. D 58 (1998) 114008

[22] J.C. Collins and A. Freund. Phys. Rev. D 59 (1999) 74009

[23] L.L. Frankfurt, A. Freund and M. Strikman. Phys. Rev. D 58 (1998) 114001
L.L. Frankfurt, A. Freund and M. Strikman. Phys. Rev. D 59 (1999) 119901

[24] X. Ji. Phys. Rev. Lett. 78 (1997) 610

[25] K. Golec-Biernat and A. Martin. Phys. Rev. D 59 (1999) 014029

[26] P.R.B. Saull, A Monte Carlo generator for deeply virtual Compton scattering at HERA, DESY, Hamburg, Germany, 1999.

[27] H1 Collaboration, C. Adloff et al., Phys. Lett. B 517 (2001) 47

[28] HERMES Collaboration, A. Airapetian et al., Phys. Rev. Lett. 87 (2001) 182001

[29] CLAS Collaboration, S. Stepanyan et al., Phys. Rev. Lett. 87 (2001) 182002

[30] A. Freund, M. McDermott and M. Strikman. Phys. Rev. D 67 (2003) 036001

[31] T. Abe. Comput. Phys. Commun. 136 (2001) 126

[32] ZEUS Collaboration, J. Breitweg et al., Eur. Phys. J. C 6 (1999) 603
ZEUS Collaboration, J. Breitweg et al.. Eur. Phys. J. C 14 (2000) 213

[33] ZEUS Collaboration, S. Chekanov et al., Eur. Phys. J. C 24 (2002) 345

[34] H1 Collaboration, C. Adloff et al., Eur. Phys. J. C 13 (2000) 371

[35] H1 Collaboration, C. Adloff et al., Phys. Lett. B 483 (2000) 360

[36] R.S. Thorne et al., In: G. Bruni, G. Iacobucci and R. Nania, Editors, Proceedings of the 9th International Workshop on Deep Inelastic Scattering (DIS 2001), Bologna, Italy (2001), pp. 405408; (hep-ph/0106075).

[37] A.D. Martin et al., Nucl. Phys. B (Proc. Suppl.) 79 (1999) 105

[38] ZEUS Collaboration, S.Chekanov et al., Phys. Lett. B 560 (2003) 7

[39] S. Catani et al.. Nucl. Phys. B 406 (1993) 187

[40] S.D. Ellis and D.E. Soper. Phys. Rev. D 48 (1993) 3160

[41] J.E. Huth et al.. In: E.L. Berger, Editor, Research Directions for the Decade, Proceedings of Summer Study on High Energy Physics, 1990, World Scientific, Singapore (1992) 134; also in preprint FERMILAB-CONF-90-249-E

[42] T. Sjöstrand. Comput. Phys. Commun. 82 (1994) 74

[43] G. Marchesini et al.. Comput. Phys. Commun. 67 (1992) 465

[44] B. Andersson et al.. Phys. Rep. 97 (1983) 31

[45] B.R. Webber. Nucl. Phys. B 238 (1984) 492

[46] M. Klasen, T. Kleinwort, G. Kramer, Eur. Phys. J. Direct C 1 (1998) 1

[47] A.D. Martin et al. Eur. Phys. C 4 (1998) 463;
A.D. Martin et al. Eur. Phys. C 14 (2000) 133

[48] M. Glück, E. Reya, A. Vogt, Pys. Rev. D 45 (1992) 3986;
M. Glück, E. Reya, A. Vogt, Pys. Rev. D 46 (1992) 1973

[49] S. Bethke. J. Phys. G 26 (2000) R27. Updated in: S. Bethke, hep-ex/0211012

[50] S. Frixione et al.. Phys. Lett. B 319 (1993) 339

[51] ZEUS Collaboration, J. Breitweg et al., Phys. Lett. B 507 (2001) 70
ZEUS Collaboration, S. Chekanov et al., Phys. Lett. B 547 (2002) 164

[52] H1 Collaboration, C. Adloff et al., Eur. Phys. J. C 19 (2001) 289

[53] CDF Collaboration, T. Affolder et al., Phys. Rev. Lett. 88 (2002) 042001